Article

# –  Bonding Interactions Generated by Halogen Oxidation of Zirconium(IV) Redox-Active Ligand Complexes

Nicole A. Ketterer, Hongjun Fan, Karen J. Blackmore, Xiaofan Yang, Joseph W. Ziller, Mu-Hyun Baik, and Alan F. Heyduk

*J. Am. Chem. Soc.*, **2008**, 130 (13), 4364-4374 • DOI: 10.1021/ja077337m



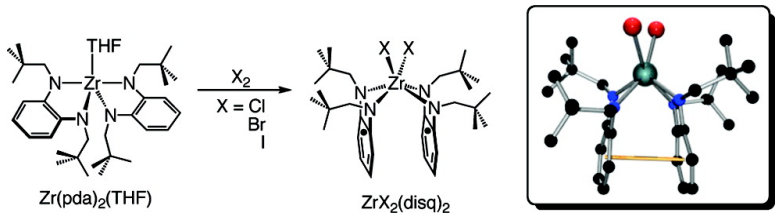


## More About This Article

Additional resources and features associated with this article are available within the HTML version:

- Supporting Information
- Links to the 6 articles that cite this article, as of the time of this article download
- Access to high resolution figures
- Links to articles and content related to this article
- Copyright permission to reproduce figures and/or text from this article

View the Full Text HTML

J|A|C|S
ARTICLES
Published on Web 03/11/2008

# $\pi^{\bullet}-\pi^{\bullet}$ Bonding Interactions Generated by Halogen Oxidation of Zirconium(IV) Redox-Active Ligand Complexes

Nicole A. Ketterer,[†] Hongjun Fan,[‡] Karen J. Blackmore,[†] Xiaofan Yang,[‡] Joseph W. Ziller,[†] Mu-Hyun Baik,*[,‡] and Alan F. Heyduk*[,†]

*Department of Chemistry, University of California, Irvine, California 92697, and Department of Chemistry & School of Informatics, Indiana University, Bloomington, Indiana 47405*

Received September 21, 2007; E-mail: aheyduk@uci.edu; mbaik@indiana.edu

***Abstract:*** The new complex, $[Zr(pda)_2]_n$ (**1**, $pda^{2-}$ = *N*,*N*′-bis(*neo*-pentyl)-ortho-phenylenediamide, $n = 1$ or 2), prepared by the reaction of 2 equiv of $pdaLi_2$ with $ZrCl_4$, reacts rapidly with halogen oxidants to afford the new product $ZrX_2(disq)_2$ (**3**, X = Cl, Br, I; $disq^-$ = *N*,*N*′-bis(*neo*-pentyl)-ortho-diiminosemiquinonate) in which each redox-active ligand has been oxidized by one electron. The oxidation products **3a**−**c** have been structurally characterized and display an unusual parallel stacked arrangement of the $disq^-$ ligands in the solid state, with a separation of ~3 Å. Density functional calculations show a bonding-type interaction between the SOMOs of the $disq^-$ ligands to form a unique HOMO while the antibonding linear combination forms a unique LUMO. This orbital configuration leads to a closed-shell-singlet ground-state electron configuration ($S = 0$). Temperature-dependent magnetism measurements indicate a low-lying triplet excited state at ~750 $cm^{-1}$. In solution, **3a**−**c** show strong $disq^-$-based absorption bands that are invariant across the halide series. Taken together these spectroscopic measurements provide experimental values for the one- and two-electron energies that characterize the $\pi$-stacked bonding interaction between the two $disq^-$ ligands.

## Introduction

Catecholate complexes of transition metal ions provide an archetype for understanding the interplay of ligand-based and metal-based redox activity.[1] Three basic oxidation states dominate the coordination chemistry of catecholate-type ligands coordinated to transition metals, the dianionic catecholate form, the monoanionic semi-quinonate form, and the neutral quinone form (eq 1). The redox potentials of these three oxidation states normally fall within the envelope of metal-centered valence changes, leading to the observation of non-innocent behavior, which have been elucidated by spectroscopic, electrochemical, and reactivity studies.[2] Molecular orbital theory predicts that the degree of ligand non-innocence derives directly from the extent of frontier orbital mixing between the ligand-based $\pi$ orbitals and the metal-based *d*-orbital manifold; this prediction has been validated in electrochemical and spectroscopic studies of $[Ru^{II}(cat)_n(bpy)_{3-n}]^{(2-2n)+}$ derivatives, where cat denotes the related catecholate, *ortho*-aminophenolate, or *ortho*-phenylenediamide ligands.[3] To further extend this construct for cooperative metal−ligand redox behavior, we have turned our efforts to the synthesis of complexes with redox-active ligands and high-valent early transition metals.[4] We surmised that the mild redox activity of *ortho*-phenylenediamide ligands might enable redox reactivity at metal centers normally incapable of further oxidation state changes.

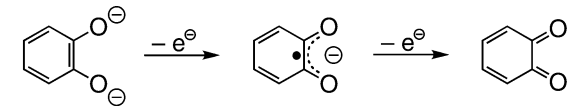

(1)

The coordination and reaction chemistry of early transition metal ions with catecholate ligands has focused on complexes of the first-row metals titanium and vanadium. The stable homoleptic titanium catecholate species, $[Ti(cat)_3]^{2-}$, is prepared by the direct action of catechol on $TiCl_4$ in acidic aqueous solutions.[5] Tris(catecholate) titanium species are stable enough to be used as structural units in the assembly of supramolecular cages in aqueous solution,[6] but oxidation studies of these systems are limited.[2] Monoanionic tris(catecholate) complexes of vanadium, $[V^{V}(cat)_3]^-$,[7] are known, as is the neutral tris(semi-quinone) complex, $V^{III}(sq)_3$.[8,9] These species react with molecular oxygen to afford vanadyl species,[10] which have been

[†] University of California.
[‡] Indiana University.

(1) (a) Hendrickson, D. N.; Pierpont, C. G. *Top. Curr. Chem.* **2004**, *234*, 63−95. (b) Chaudhuri, P.; Verani, C. N.; Bill, E.; Bothe, E.; Weyhermuller, T.; Wieghardt, K. *J. Am. Chem. Soc.* **2001**, *123*, 2213−2223.
(2) (a) Zanello, P.; Corsini, M. *Coord. Chem. Rev.* **2006**, *250*, 2000−2022. (b) Pierpont, C. G. *Coord. Chem. Rev.* **2001**, *219*−*221*, 415−433. (c) Pierpont, C. G. *Coord. Chem. Rev.* **2001**, *216*−*217*, 99−125.
(3) Haga, M.; Dodsworth, E. S.; Lever, A. B. P. *Inorg. Chem.* ***1986***, *25*, 447−453.
(4) (a) Haneline, M. R.; Heyduk, A. F. *J. Am. Chem. Soc.* **2006**, *128*, 8410−8411. (b) Blackmore, K. J.; Ziller, J. W.; Heyduk, A. F. *Inorg. Chem.* **2005**, *44*, 5559−5561.
(5) Borgias, B. A.; Cooper, S. R.; Koh, Y. B.; Raymond, K. N. *Inorg. Chem.* **1984**, *23*, 1009−1016.
(6) Caulder, D. L.; Raymond, K. N. *Acc. Chem. Res.* **1999**, *32*, 975−982.
(7) Cooper, S. R.; Koh, Y. B.; Raymond, K. N. *J. Am. Chem. Soc.* **1982**, *104*, 5092−102.


**10.1021/ja077337m CCC: $40.75** 

implicated in catechol dioxygenase reactions.[11] These oxidation reactions are enabled, at least partially, by the redox activity of the catecholate ligands; however, the oxidation reactions also lead to coordinative instability via ejection of a quinone ligand from the transition metal coordination sphere.

One strategy to enhance the stability of electron-poor transition metals with one-electron oxidized semiquinone- or two-electron oxidized quinone-type ligands is to replace the oxygen donor atoms with nitrogen donor atoms. In the reduced, catecholate form, the ligand coordinates through strong $\pi$-donor amide groups, whereas in the oxidized, quinone form, the ligand coordinates through strong $\sigma$-donor imine groups. These imines are better donors for transition metals than their ketone oxygen counterparts, which should increase the stability of metal complexes with ligands in the quinone oxidation state.

*ortho*-Phenylenediamine ligands have received attention for early and mid-transition metal ions since they offer an analogous coordination geometry to catechols in addition to the possibility for steric control through *N*-functionalization. The *N*,*N*′-bis(trimethylsilyl)-*ortho*-phenylenediamide ligand has been used to stabilize various complexes of molybdenum and tungsten with metal−ligand multiple bonds;[12] however, we have found for zirconium complexes of this ligand that silyl migration occurs readily in reactions with reducible nitrogen-containing molecules.[13] Both *N*-alkyl and *N*-alkylsilyl phenylenediamine derivatives have been used to prepare $d^0$ metal complexes as catalysts in olefin polymerization[14] and in hydroamination,[15] so we envisioned that *N*-alkylated derivatives should coordinate strongly to zirconium without competing silyl migration reactions. In the reduced catecholate form, *N*,*N*′-bis(*neo*-pentyl)-*ortho*-phenylenediamide ($pda^{2-}$, eq 2) coordinates to zirconium with two anionic amide nitrogen atoms. One-electron oxidation to the semi-quinone form, *N*,*N*′-bis(*neo*-pentyl)-*ortho*-diiminosemiquinonate ($disq^-$), renders a ligand that is anionic, analogous to the well-established $\beta$-diketiminate family of ligands.[16,17] Two-electron oxidation of a coordinated $pda^{2-}$ ligand gives access to the quinone form, *N*,*N*′-bis(*neo*-pentyl)-*ortho*-diiminoquinone (diq), which is neutral and isoelectronic with a chelating α-diketimine ligand.[18]

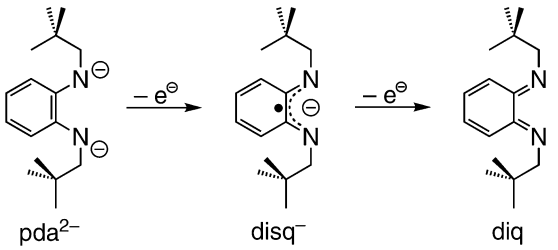


(2)

This paper reports the first study of the oxidative reactivity of zirconium(IV) complexes with redox-active $pda^{2-}$ ligands. The homoleptic $Zr(pda)_2$ fragment (**1a**) dimerized in the solid state and readily added basic solvents like tetrahydrofuran (THF) to form $Zr(pda)_2(THF)$ (**2**). Oxidation of **1** or **2** with halogen reagents proceeded smoothly to afford zirconium(IV) halide complexes $ZrX_2(disq)_2$ (**3a**, X = Cl; **3b**, X = Br; **3c**, X = I; in which halide addition occurred at the metal center with each redox-active ligand getting oxidized to the diimino-semiquinone form.

The electronic structure of complexes **3a**−**c** is of interest because the coordination sphere of each complex contains two monoanionic, formally open-shell, $disq^-$ ligands. As such, experimental and theoretical methods have been used to probe the electronic structure of **3a**−**c**. Both experiment and theory support a diamagnetic ground state for complexes **3a**−**c**. Whereas we are not aware of any examples of ligand-based unpaired electrons coupling antiferromagnetically across a $d^0$-metal center, intermolecular $\pi^{\bullet}$−$\pi^{\bullet}$ interactions have been reported for phenalenyl radicals,[19] molybdenum semi-quinone radicals,[20] and various metal-coordinated TCNE radicals.[21] In this manuscript, we report experimental and theoretical evidence that an intramolecular $\pi^{\bullet}$−$\pi^{\bullet}$ interaction leads to a closed-shell singlet ground-state electron configuration for complexes **3a**−**c**.

## Experimental Section

**General Procedures.** The complexes described below are air- and moisture-sensitive, necessitating that manipulations be carried out under an inert atmosphere of argon or nitrogen gas using standard Schlenk, vacuum-line, and glovebox techniques. Hydrocarbon solvents were sparged with argon and then dried and deoxygenated by passage through activated alumina columns and Q5, respectively. Ethereal solvents were sparged with argon and then dried by passage through double-activated alumina columns. To test for effective oxygen and water removal, the solvents were treated with a few drops of a purple solution of sodium benzophenone ketyl in THF. The metal salt $ZrCl_4$ was used as received

(8) (a) Buchanan, R. M.; Downs, H. H.; Shorthill, W. B.; Pierpont, C. G.; Kessel, S. L.; Hendrickson, D. N. *J. Am. Chem. Soc.* **1978**, *100*, 4318−4320. (b) Riechel, T. L.; Sawyer, D. T. *Inorg. Chem.* **1975**, *14*, 1869−1875.

(9) This species may be more accurately described as a vanadium(V) complex with two catecholate and one semiquinonate ligands, see (a) Chun, H.; Verani, C. N.; Chaudhuri, P.; Bothe, E.; Bill, E.; Weyhermuller, T.; Wieghardt, K. *Inorg. Chem.* **2001**, *40*, 4157−4166. (b) Cass, M. E.; Gordon, N. R.; Pierpont, C. G. *Inorg. Chem.* **1986**, *25*, 3962−3967.

(10) Cass, M. E.; Greene, D. L.; Buchanan, R. M.; Pierpont, C. G. *J. Am. Chem. Soc.* **1983**, *105*, 2680−2686.

(11) (a) Yin, C. X.; Finke, R. G. *J. Am. Chem. Soc.* **2005**, *127*, 9003−9013. (b) Yin, C. X.; Finke, R. G. *J. Am. Chem. Soc.* **2005**, *127*, 13988−13996.

(12) (a) Hayton, T. W.; Boncella, J. M.; Scott, B. L.; Abboud, K. A.; Mills, R. C. *Inorg. Chem.* **2005**, *44*, 9506−9517. (b) Ison, E. A.; Cameron, T. M.; Abboud, K. A.; Boncella, J. M. *Organometallics* **2004**, *23*, 4070−4076.

(13) Heyduk, A. F.; Blackmore, K. J.; Ketterer, N. A.; Ziller, J. W. *Inorg. Chem.* **2005**, *44*, 468−470.

(14) (a) Tabernero, V.; Cuenca, T. *Eur. J. Inorg. Chem.* **2005**, 338−346. (b) Sanz, M.; Cuenca, T.; Galakhov, M.; Grassi, A.; Bott, R. K. J.; Hughes, D. L.; Lancaster, S. J.; Bochmann, M. *Organometallics* **2004**, *23*, 5324−533. (c) Daniele, S.; Hitchcock, P. B.; Lappert, M. F.; Merle, P. G. *J. Chem. Soc., Dalton Trans.* **2001**, 13−19. (d) Kalai, K.; Tilley, T. D.; Aoyagi, K.; Gantzel, P. K. *Organometallics* **1996**, *15*, 923−927.

(15) Kim, Y. K.; Livinghouse, T.; Bercaw, J. E. *Tetrahedron Lett.* **2001**, *42*, 2933−2935.

(16) For examples of $\beta$-diketiminate complexes of zirconium, see (a) Basuli, F.; Kilgore, U. J.; Brown, D.; Huffman, J. C.; Mindiola, D. J. *Organometallics* **2004**, *23*, 6166−6175. (b) Franceschini, P. L.; Morstein, M.; Berke, H.; Schmalle, H. W. *Inorg. Chem.* **2003**, *42*, 7273−7282. (c) Qian, B.; Scanlon, W. J.; Smith, M. R.; Motry, D. H. *Organometallics* **1999**, *18*, 1693−1698. (d) Rahim, M.; Taylor, N. J.; Xin, S.; Collins, S. *Organometallics* **1998**, *17*, 1315−1323.

(17) The electronic properties of the $disq^-$ ligand are dependent on the localization of the odd electron. If the odd electron is localized exclusively in the phenyl ring the ligand would be isoelectronic with a $\beta$-diketiminate; however, our computational results suggest significant radical character on the nitrogen atoms, which makes the isoelectronic label inappropriate.

(18) For a recent example of the addition of an α-diketimine to zirconium, see De Waele, P.; Jazdzewski, B. A.; Klosin, J.; Murray, R. E.; Theriault, C. N.; Vosejpka, P. C.; Petersen, J. L. *Organometallics* **2007**, *26*, 3896−3899.

(19) (a) Small, D.; Rosokha, S. V.; Kochi, J. K.; Head-Gordon, M. *J. Phys. Chem. A* **2005**, *109*, 11261−11267. (b) Small, D.; Zaitsev, V.; Jung, Y.; Rosokha, S. V.; Head-Gordon, M.; Kochi, J. K. *J. Am. Chem. Soc.* **2004**, *126*, 13850−13858.

(20) (a) Pierpont, C. G.; Buchanan, R. M. *Coord. Chem. Rev.* **1981**, *38*, 45−87. (b) Pierpont, C. G.; Buchanan, R. M. *J. Am. Chem. Soc.* **1975**, *97*, 4912−4917.

(21) (a) Lü, J.-M.; Rosokha, S. V.; Kochi, J. K. *J. Am. Chem. Soc.* **2003**, *125*, 12161−12171. (b) Novoa, J. J.; Lafuente, P.; Del Sesto, R. E.; Miller, J. S. *Angew. Chem. Int. Ed.* **2001**, *40*, 2540−2545. (c) Novoa, J. N.; Ribas-Arino, J.; Shum, W. W.; Miller, J. S. *Inorg. Chem.* **2007**, *46*, 103−107.

from Alfa-Aesar. Purification of elemental bromine (Acros) and iodine (EM Science) was achieved by distillation from $P_2O_5$ and by sublimation, respectively. Phenyliodide dichloride[22] and *N*,*N*′-di-*neo*-pentyl-1,2-phenylenediamine ($pdaH_2$)[23] were prepared according to published procedures.

**Physical Measurements.** NMR spectra were collected on Bruker Avance 400, 500, and 600 MHz spectrometers in dry, degassed benzene-$d_6$. $^1$H NMR spectra were referenced to TMS using the residual proteo impurities of the solvent; $^{13}$C NMR spectra were referenced to TMS using the natural abundance $^{13}$C impurities of the solvent. All chemical shifts are reported using the standard notation in parts per million; positive chemical shifts are to a higher frequency from the given reference. Infrared spectra were recorded as KBr pellets with a Perkin-Elmer Spectrum One FTIR spectrophotometer. Electronic absorption spectra were recorded with a Perkin-Elmer Lambda 800 UV−vis spectrophotometer. Magnetic measurements of solid materials were recorded at UC San Diego on a Quantum Design SQUID magnetometer at 10 kOe between 5 and 400 K. Pascals' constants were used to correct the magnetic susceptibility data. Elemental analyses were provided by Desert Analytics. While acceptable analyses were obtained for all reported compounds, due to their extreme sensitivity, analysis results were often irreproducible.

**Preparation of $[Zr(pda)_2]_n$ ($n = 1$, 1a; $n = 2$, 1b).** In a nitrogen-filled glovebox, $pdaLi_2$ (3.30 g, 12.7 mmol, 1.95 equiv) was suspended in 40 mL of benzene. $ZrCl_4$ (1.52 g, 6.5 mmol, 1 equiv) was added, and the reaction was then stirred for 14 h. The reaction became dark brownish red, and white precipitate formed which was removed by filtration and washed with benzene. The organics were combined, and the solvent was removed in vacuo to provide **1** (3.14 g, 82% yield). X-ray quality crystals of **1b** were obtained by dissolving the compound in toluene and cooling to −35 °C. Anal. Calcd for $C_{32}H_{52}N_4Zr$: C, 65.81; H, 8.97; N, 9.59. Found: C, 65.91; H, 8.57; N, 9.59. IR (KBr) $\nu$/cm$^{-1}$: 736, 1044, 1200, 1253, 1314, 1362, 1475, 1513, 1600, 2865, 2951. UV/vis ($C_6H_6$) $\lambda_{max}$/nm ($\epsilon$/M$^{-1}$ cm$^{-1}$): 361 (10422). $^1$H NMR (500 MHz) $\delta$/ppm: 0.85 (s, 36H, $^t$Bu), 3.31 (s, 8H, $CH_2$), 7.08 (m, 4H, Ar−H), 7.16 (m, 4H, Ar−H). $^{13}$C NMR (125.7 MHz) $\delta$/ppm: 28.51 ($CH_2C(CH_3)_3$), 33.79 ($CH_2C(CH_3)_3$), 62.39 ($CH_2C(CH_3)_3$), 116.60 (aryl−C), 122.09 (aryl−C), 128.40 (aryl−C).

**Preparation of $Zr(pda)_2(THF)$ (2).** In a nitrogen filled glovebox, $pdaLi_2$ (0.3087 g, 1.186 mmol, 1 equiv) was suspended in $Et_2O$ (40 mL), and the solution was cooled in a $N_2$ cold well. $ZrCl_4(THF)_2$ (0.2254 g, 0.5978 mmol, 0.5 equiv) was added to the cold solution. The reaction was warmed to room temperature and was then stirred for 14 h. At this time a white solid had precipitated, and the solution was dark brownish red. The solution was filtered and the solvent removed in vacuo. Orange crystals were grown from a pentane/THF mixture cooled to −35 °C to provide **2** (0.80 g, 20.5%). Anal. Calcd for $C_{36}H_{60}N_4OZr$: C, 65.90; H, 9.22; N, 8.54. Found: C, 65.37; H, 8.83; N, 8.57. $^1$H NMR (500 MHz) $\delta$/ppm: 0.89 (s, 36H, $^t$Bu), 1.22 (m, 4H, THF−$CH_2$), 3.47 (s, 8H, $CH_2$), 3.57 (m, 4H, THF−$OCH_2$), 7.09 (m, 4H, aryl−H), 7.11 (m, 4H, aryl−H). $^{13}$C NMR (125.7 MHz) $\delta$/ppm: 5.32 (THF−$CH_2$), 28.87 ($CH_2C(CH_3)_3$), 34.63 ($CH_2C(CH_3)_3$), 60.60 ($CH_2C(CH_3)_3$), 71.67 (THF−$OCH_2$), 114.38 (aryl−C), 120.15 (aryl−C), 136.01 (aryl−C).

**Preparation of $ZrCl_2(disq)_2$ (3a).** In a nitrogen filled glovebox, compound **1** (0.11 g, 0.19 mmol, 1 equiv) was dissolved in 15 mL of diethyl ether. The solution was frozen in a liquid nitrogen cold well. Upon thawing, $PhICl_2$ (0.050 g, 0.20 mmol, 1 equiv) was added to the solution. A dark green color was immediately observed. The mixture was stored at −35 °C overnight, and dark purple crystals of **3a** (0.04 g, 25% yield) suitable for X-ray diffraction were deposited. Reprocessing the mother liquor raised the overall yield to 59%. Anal. Calcd for $C_{36}H_{62}N_4OZrCl_2$: C, 59.01; H, 8.30; N, 8.10. Found: C, 58.62; H, 8.61; N, 8.24. IR (KBr) $\nu$/cm$^{-1}$: 561, 735, 771, 1041, 1162, 1237, 1268, 1263, 1435, 1473, 1517, 1594, 2866, 2952. UV/vis ($C_6H_6$) $\lambda_{max}$/nm ($\epsilon$/M$^{-1}$ cm$^{-1}$): 443 (2579), 660 (7845). $^1$H NMR (500 MHz) $\delta$/ppm: 1.01 (*s*, 36H, $^t$Bu), 3.23 (*d*, 4H, $CH_2$, $^3J_{HH} = 11.5$), 4.78 (*d*, 4H, $CH_2$, $^3J_{HH} = 12.0$), 5.74 (*m*, 4H, aryl−H), 6.06 (*m*, 4H, aryl−H). $^{13}$C NMR (100.6 MHz) $\delta$/ppm: 29.15 ($CH_2C(CH_3)_3$), 36.13 (($CH_2C(CH_3)_3$), 61.70 ($CH_2C(CH_3)_3$), 116.78 (aryl−C), 122.24 (aryl−C), 124.97 (aryl−C).

**Preparation of $ZrBr_2(disq)_2$ (3b).** Complex **3b** was prepared similarly to **3a** from $Br_2$ (18 $\mu$L, 0.35 mmol, 1 equiv) and **1** (0.22 g, 0.35 mmol, 1 equiv) to give the product as a purple crystalline solid (0.091 g, 60% yield). Anal. Calcd for $C_{36}H_{62}N_4OZrBr_2$: C, 52.86; H, 7.64; N, 6.85. Found: C, 52.17; H, 7.42; N, 7.46. IR (KBr) $\nu$/cm$^{-1}$: 560, 735, 1041, 1161, 1266, 1363, 1434, 1474, 1517, 1594, 2865, 1958. UV/vis ($C_6H_6$) $\lambda_{max}$/nm ($\epsilon$/M$^{-1}$ cm$^{-1}$): 453 (2540), 653 (7533). $^1$H NMR (400 MHz) $\delta$/ppm: 1.03 (*t*, 36H, $^t$Bu), 3.23 (*d*, 4H, $CH_2$, $^3J_{HH} = 12.2$), 5.01 (*d*, 4H, $CH_2$, $^3J_{HH} = 12.0$), 5.72 (*m*, 4H, aryl−H), 6.07 (*m*, 4H, aryl−H). $^{13}$C NMR (100.6 MHz) $\delta$/ppm: 29.33 ($CH_2C(CH_3)_3$), 36.06 ($CH_2C(CH_3)_3$), 61.80 ($CH_2C(CH_3)_3$), 117.65 (aryl−C), 122.43 (aryl−C), 125.33 (aryl−C).

**Preparation of $ZrI_2(disq)_2$ (3c).** Complex **3c** was prepared similarly to **3a** from $I_2$ (0.13 g, 0.053 mmol, 1 equiv) and **1** (0.29 g, 0.050 mmol, 1 equiv) to give the product as a purple crystalline solid (0.16 g, 51% yield). Anal. Calcd for $C_{36}H_{62}N_4OZrI_2$: C, 47.41; H, 6.85; N, 6.14. Found: C, 47.55; H, 6.66; N, 6.86. IR (KBr) $\nu$/cm$^{-1}$: 559, 756, 1041, 1157, 1266, 1357, 1436, 1475, 1518, 1616, 2866, 2957. UV/vis ($C_6H_6$) $\lambda_{max}$/nm ($\epsilon$/M$^{-1}$ cm$^{-1}$): 460 (2921), 652 (8269). $^1$H NMR (500 MHz) $\delta$/ppm: 1.03 (*t*, 36H, $^t$Bu), 3.25 (*d*, 4H, $CH_2$, $^3J_{HH} = 12.1$), 5.26 (*d*, 4H, $CH_2$, $^3J_{HH} = 12.2$), 5.72 (*m*, 4H, aryl-H), 6.07 (*m*, 4H, aryl-H). $^{13}$C NMR (100.6 MHz) $\delta$/ppm: 29.41 ($CH_2C(CH_3)_3$), 36.00 ($CH_2C(CH_3)_3$), 61.87 ($CH_2C(CH_3)_3$), 117.69 (aryl−C), 125.56 (aryl−C), 142.34 (aryl−C).

**General Details of X-ray Data Collection and Reduction.** X-ray diffraction data were collected on a Bruker CCD platform diffractometer equipped with a CCD detector. Measurements were carried out at 163 K using Mo K$\alpha$ ($\lambda = 0.71073$ Å) radiation, which was wavelength selected with a single-crystal graphite monochromator. The SMART[24] program package was used to determine unit-cell parameters and for data collection. The raw frame data were processed using SAINT[25] and SADABS[26] to yield the reflection data files. Subsequent calculations were carried out using the SHELXTL[27] program suite. Analytical scattering factors for neutral atoms were used throughout the analyses.[28] Thermal ellipsoid plots were generated using the XP program within the SHELXTL suite. Diffraction data for **1b·3C$_6$H$_5$Me**, **2**, and **3a−c·OEt$_2$** are shown in Table 1.

**Computational Details.** All calculations were carried out using density functional theory (DFT) and MP2 theory as implemented in the Jaguar 6.0 suite,[29] except for TDDFT calculations (vide infra). All geometries were optimized with the BP86[30] functional and the 6-31G** basis set. For Zr, the Los Alamos LACVP basis[31] including effective core potentials was used. The energies of the optimized structures were reevaluated by additional single-point calculations using Dunning's correlation-consistent triple-$\zeta$ basis set[32] cc-pVTZ(-f). For Zr we used

(22) Lucas, H. J.; Kennedy, E. R. In *Organic Syntheses*; Horning, E. C., Ed.; Wiley: New York, 1955; Vol. 3, pp 482−483.
(23) Danièle, S.; Drost, C.; Gehrhus, B.; Hawkins, S. M.; Hitchcock, P. B.; Lappert, M. F.; Merle, P. G.; Bott, S. G. *J. Chem. Soc., Dalton Trans.* **2001**, 3179−3188.
(24) *SMART Software Users Guide*, Version 5.1; Bruker Analytical X-Ray Systems, Inc.: Madison, WI, 1999.
(25) *SAINT Software Users Guide*, Version 6.0; Bruker Analytical X-Ray Systems, Inc.; Madison, WI, 1999.
(26) Sheldrick, G. M. *SADABS*, Version 2.05; Bruker Analytical X-Ray Systems, Inc.: Madison, WI, 2001.
(27) Sheldrick, G. M. *SHELXTL*, Version 6.12; Bruker Analytical X-Ray Systems, Inc.: Madison, WI, 2001.
(28) *International Tables for X-Ray Crystallography*; Kluwer Academic Publishers: Dordrecht, 1992; Vol. C.
(29) *Jaguar*, 6.0 ed.; Schrödinger, L.L.C.: Portland, OR, 1991−2005.
(30) (a) Becke, A. D. *Phys. Rev. A* **1988**, *38*, 3098−3100. (b) Perdew, J. P. *Phys. Rev. B* **1986**, *33*, 8822−8824.
(31) Hay, P. J.; Wadt, W. R. *J. Chem. Phys.* **1985**, *82*, 270−283.

***Table 1.*** Crystal Data Collection and Refinement Parameters

| | $[Zr(pda)_2]_2 \cdot 3$ PhMe (**1b**·3 PhMe) | $Zr(pda)_2(THF)$ (**2**) | $ZrCl_2(disq)_2 \cdot Et_2O$ (**3a**·$Et_2O$) | $ZrBr_2(disq)_2 \cdot Et_2O$ (**3b**·$Et_2O$) | $ZrI_2(disq)_2 \cdot Et_2O$ (**3c**·$Et_2O$) |
|---|---|---|---|---|---|
| empirical formula | $C_{85}H_{128}N_8Zr_2$ | $C_{36}H_{60}N_4OZr$ | $C_{36}H_{62}Cl_2N_4OZr$ | $C_{36}H_{62}Br_2N_4OZr$ | $C_{36}H_{62}Cl_{0.70}I_{1.30}N_4OZr$ |
| formula weight | 1444.39 | 656.10 | 729.02 | 817.94 | 847.90 |
| crystal system | triclinic | monoclinic | monoclinic | monoclinic | monoclinic |
| space group | $P\bar{1}$ | $C2/c$ | $P2_1$ | $P2_1$ | $P2_1/c$ |
| $a$, Å | 11.0057(10) | 29.745(5) | 9.9356(8) | 10.0490(9) | 11.7217(10) |
| $b$, Å | 11.7715(11) | 14.043(2) | 14.7888(12) | 14.7969(13) | 17.3104(15) |
| $c$, Å | 16.1248(15) | 20.461(3) | 13.7171(12) | 13.7501(12) | 20.0003(17) |
| α, deg | 78.922(2) | 90 | 90 | 90 | 90 |
| $\beta$, deg | 79.575(2) | 122.277(2) | 100.9610(10) | 101.533(2) | 100.315(2) |
| $\gamma$, deg | 75.362(2) | 90 | 90 | 90 | 90 |
| $V$, Å$^3$ | 1964.2(3) | 7226.3(19) | 1978.8(3) | 2003.3(3) | 3992.6(6) |
| $Z$ | 1 | 8 | 2 | 2 | 4 |
| reflns collected | 25326 | 38238 | 21867 | 22284 | 43644 |
| independent reflns | 9575 | 8840 | 9573 | 9751 | 9897 |
| | $R_{int} = 0.0239$ | $R_{int} = 0.0436$ | $R_{int} = 0.0184$ | $R_{int} = 0.0234$ | $R_{int} = 0.0332$ |
| GOF | 1.055 | 1.053 | 1.054 | 1.080 | 1.069 |
| $R1$/w$R2$ [$I > 2\sigma(I)$] | 0.0268/0.0680 | 0.0314/0.0673 | 0.0221/0.0563 | 0.0368/0.1043 | 0.0390/0.1017 |
| $R1$/w$R2$ (all data) | 0.0312/0.0714 | 0.0555/0.0778 | 0.0233/0.0570 | 0.0399/0.1066 | 0.0518/0.1097 |

a modified version of LACVP, designated as LACV3P, in which the exponents were decontracted to match the triple-ζ quality basis. Although the ubiquitous B3LYP[33] functional is reliable for modeling even transition metal complexes, it tends to overestimate the contribution of exchange[34] energy, thus, possibly leading to an artificial preference of the triplet spin states. Because one of the main interests of this work is concerned with the thermodynamic stabilities of different spin states, we purposely chose BP86 instead of B3LYP. Exploratory calculations showed that B3LYP-based geometry optimizations gave essentially identical structures. Vibrational frequency calculations based on analytical second derivatives at the BP86/6-31G** (LACVP) level of theory were carried out using Jaguar with simplified models (all *neo*-pentyl groups were simplified to $CH_3$) to derive the zero point vibrational energy (ZPVE) and entropy corrections at room temperature utilizing unscaled frequencies. By entropy we refer specifically to the vibrational/rotational/translational entropy of the solute(s); the entropy of the solvent is implicitly included in the dielectric continuum model. Solvation energies were evaluated by a self-consistent reaction field (SCRF) approach based on numerical solutions of the Poisson−Boltzmann equation.[35] These calculations were carried out at the optimized gas-phase geometry employing the dielectric constant of $\epsilon = 2.284$ (benzene). As is the case for all continuum models, the solvation energies are subject to empirical parameters for the atomic radii used to generate the solute surface. We employ the standard set of radii for H (1.150 Å), C (1.900 Å), N (1.600 Å), O (1.600 Å), Cl (1.974 Å), Br (2.095 Å), I (2.250 Å), and Zr (1.562 Å). The broken symmetry (BS) orbital approach[36] using Boys-localized orbitals as initial guesses was employed to model antiferromagnetically (AF) coupled states. As pointed out repeatedly in our unrelated previous work,[37] modeling AF coupling is difficult and requires careful monitoring of Mulliken spin populations and the frontier molecular orbitals to ensure convergence to plausible states. Time-dependent DFT calculations using the LB94 functional[38] were used to compute electronic excitation energies and compared to experiments. We used both the DFT- and MP2-optimized geometries for these calculations. All calculations were carried out using the Amsterdam Density Functional (ADF 2006) package,[39] utilizing the triple-ζ basis set (ZORA/TZP) and the frozen-core approximation. Relativistic effect was evaluated at the scalar ZORA level of theory.[40]

***Scheme 1***

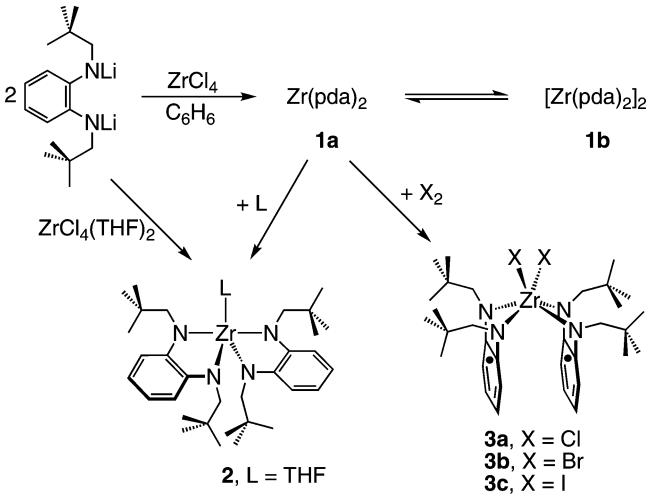


## Results

**Synthesis and Characterization.** Scheme 1 summarizes the coordination and redox reactivity of the $pda^{2-}$ ligand coordinated to zirconium ($pda^{2-}$ = *N*,*N*′-bis(*neo*-pentyl)-*ortho*-phenylenediamide). The dark red complex, $[Zr(pda)_2]_n$ (**1a**, $n = 1$; **1b**, $n = 2$), was prepared in 82% yield from benzene solutions of $ZrCl_4$ and 2 equiv of $pdaLi_2$, which was prepared by the deprotonation of $pdaH_2$ with *n*BuLi. The $^1$H NMR spectrum of **1a** is indicative of a symmetric coordination environment about the zirconium center in solution. Notably, the methylene protons of the *neo*-pentyl groups were observed as a singlet resonance at 3.31 ppm, while the two aromatic protons resonated as multiplets at 7.08 and 7.16 ppm. The $^{13}$C NMR spectrum for **1a** is simple, displaying only three aromatic resonances and three aliphatic resonances. Variable temperature $^1$H NMR studies in

(32) Dunning, T. H. *J. Chem. Phys.* **1989**, *90*, 1007−1023.
(33) (a) Becke, A. D. *J. Chem. Phys.* **1993**, *98*, 5648−5652. (b) Lee, C. T.; Yang, W. T.; Parr, R. G. *Phys. Rev. B* **1988**, *37*, 785−789.
(34) Reiher, M.; Salomon, O.; Hess, B. A. *Theor. Chem. Acc.* **2001**, *107*, 48−55.
(35) Marten, B.; Kim, K.; Cortis, C.; Friesner, R. A.; Murphy, R. B.; Ringnalda, M. N.; Sitkoff, D.; Honig, B. *J. Phys. Chem.* **1996**, *100*, 11775−11788.
(36) Noodleman, L. *J. Chem. Phys.* **1981**, *74*, 5737−5743.
(37) (a) Baik, M.-H.; Gherman, B. F.; Friesner, R. A.; Lippard, S. J. *J. Am. Chem. Soc.* **2002**, *124*, 14608−14615. (b) Yang, X.; Baik, M. H. *J. Am. Chem. Soc.* **2004**, *126*, 13222−13223. (c) Yang, X.; Baik, M.-H. *J. Am. Chem. Soc.* **2006**, *128*, 7476−7485.
(38) van Leeuwen, R.; Baerends E. J. *Phys. Rev. A* **1994**, *49*, 2421−2431.
(39) te Velde, G. T.; Bickelhaupt, F. M.; Baerends, E. J.; Guerra, C. F.; Van Gisbergen, S. J. A.; Snijders, J. G.; Ziegler, T. *J. Comput. Chem.* **2001**, *22*, 931−967.
(40) van Lenthe, E.; van Leeuwen, R.; Baerends, E. J.; Snijders, J. G. *Int. J. Quantum Chem.* **1996**, *57*, 281−293.

toluene-$d_8$ revealed no significant line broadening between −70 and +100 °C. The solution NMR data is consistent with a four-coordinate, $D_{2d}$-symmetric structure for **1a**, as observed for the related zirconium complex, Zr[1,2-$(Me_3SiN)_2C_6H_3$]$_2$.[13]

Lewis basic solvents such as THF readily coordinate to the zirconium center of **1a** to provide a new five-coordinate species, Zr$(pda)_2$(THF), **2**. Red solutions of **1a** lightened to orange-yellow upon addition of a few drops of THF. $^1$H NMR spectra of the residue isolated after solvent removal showed the incorporation of one THF molecule into the coordination sphere as evidenced by resonances at 1.22 and 3.57 ppm. While a downfield shift of 0.16 ppm was observed for the methylene protons of the $pda^{2-}$ ligand, very little shift was observed for the aromatic resonances of the $pda^{2-}$ ligand relative to **1a**. Compound **2** also was prepared directly from 2 equiv of $pdaLi_2$ and $ZrCl_4(THF)_2$.

Exposure of **1a** or **2** to halogen oxidants resulted in a reaction to afford a product with the formula $ZrX_2(disq)_2$ (**3a**, X = Cl; **3b**, X = Br; **3c**, X = I; $disq^-$ = *N*,*N*′-di-*neo*-pentyl-1,2-diimino-semiquinonate). In a typical experiment, upon thawing of a diethyl ether solution of **1**, 1 equiv of crystalline iodine was added to the solution, which produced a color change from red-orange to dark green. The reaction mixture was placed in a −35 °C freezer and was periodically removed from the freezer and shaken over the span of 1 h. The reaction mixture was stored in the freezer overnight before the purple crystalline product, $ZrI_2(disq)_2$ (**3c**), was collected by filtration. Analogous procedures using $PhICl_2$ and $Br_2$ were used to prepare the chloride (**3a**) and bromide (**3b**) complexes, respectively.

NMR spectroscopic signatures for **3a**−**c** clearly distinguished these products from **1** and **2**. The $^1$H NMR spectra of **3a**−**c** displayed proton resonances that were shifted upfield into the olefinic region ($\delta$ 5.7−6.1 ppm), consistent with loss of aromaticity upon oxidation of the $pda^{2-}$ ligand to the $disq^-$ state. The methylene protons of the $disq^-$ ligands resonated as a diasteriotopic pair with a well-defined $^2J_{HH}$ coupling constant of 12 Hz. Across the halide series one methylene resonance consistently appeared at 3.23 ppm while the second methylene resonance shifted with the change in halogen ligand, from 4.78 (**3a**), to 5.01 (**3b**), to 5.26 (**3c**) ppm.

The intense color change associated with the formation of **3a**−**c** prompted an investigation of the electronic absorption spectra of these complexes. Dissolution of purple crystals of **3a**−**c** in benzene gave blue-green solutions with three intense absorptions in the visible range of the spectrum.[41] In **3a** these absorptions were observed at 443 nm ($\epsilon$ = 2600 $M^{-1}$ $cm^{-1}$) and as an overlapping pair at approximately 660 nm ($\epsilon$ = 7800 $M^{-1}$ $cm^{-1}$) and 730 nm ($\epsilon$ = 7400 $M^{-1}$ $cm^{-1}$); upon substitution of bromide and iodide a small red-shift (<20 nm) was observed for the high-energy band, while no significant shift (<10 nm) was observed for the lower-energy bands. Absorption spectra taken in MeCN did not show an appreciable shift in the absorption maxima listed above. On the basis of the intensity of these low-energy transitions, the lack of a dependence on halide ligand, and by comparison of the spectra for **3a**−**c**, to those of other transition-metal semi-quinone complexes,[1b] these absorptions may be assigned as LLCT transitions between the $disq^-$ ligands.

(41) Removal of the solvent from these blue-green solutions gave back a purple microcrystalline solid.

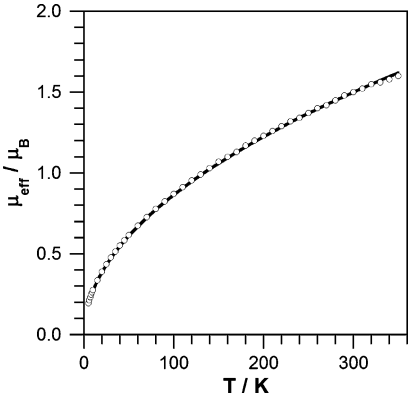


***Figure 1.*** Temperature-dependent magnetic susceptibility of $ZrCl_2(disq)_2$ (**3a**). The best fit to the data was obtained assuming only a contribution from TIP (945 × $10^{-6}$ emu).

To further elucidate the electronic structure of **3a**−**c**, variable temperature magnetic susceptibility measurements were conducted. Microcrystalline samples of **3a**−**c**, obtained after three successive recrystallizations,[42] were examined in a SQUID magnetometer from 4 to 350 K. Figure 1 shows a plot of effective magnetic moment ($\mu_B$) as a function of temperature for **3a**; super-imposable data were obtained for **3b** and **3c** (see Supporting Information). At low temperatures, the magnetic susceptibility approached zero, consistent with a singlet ground state. As the temperature was raised to 350 K a steady increase to 1.6 $\mu_B$ was measured, which is significantly lower than the spin-only magnetic susceptibility expected for two unpaired electrons (2.83 $\mu_B$). The data was fit assuming only a contribution from temperature-independent paramagnetism ($\chi_{TIP}$ = 945 × $10^{-6}$ emu). The $\chi_{TIP}$ observed for **3a**−**c** derives from mixing of the lowest-energy, triplet excited state into the singlet ground state. If the degree of mixing, and thus the magnitude of $\chi_{TIP}$, is inversely proportional to the energy difference between these two spin states, an estimated energy gap, $\Delta E_{ST}$ = 1059 K = 735 $cm^{-1}$, between the singlet ground state and the triplet excited state was obtained using eq 3 ($g$ = 2.0, $S$ = 1).[43]

$$\chi_{TIP} = \frac{N_A g^2 \mu_B{}^2}{3k_B(\Delta E_{ST})} S(S+1) \qquad (3)$$

**Structural Studies.** X-ray crystallographic studies showed that in the solid state two molecules of **1a** dimerize to form $[Zr(pda)_2]_2$ (**1b**). Dark red crystals of **1b** were grown from chilled toluene solutions of **1a**. Figure 2 shows a thermal ellipsoid plot of the dimer structure as determined by X-ray diffraction studies; selected bond lengths and angles can be found in Table 2. Four nitrogen atoms coordinate to each zirconium center along with an aryl ring of a $pda^{2-}$ ligand from the adjacent zirconium center. Four Zr—C distances in the 2.50−2.72 Å range suggest that the aryl group is best described as an $\eta^4$, four-electron donor to the zirconium center. Coordination of these four carbon atoms to the zirconium center disrupts the ring $\pi$ system, which is reflected in a 0.024 Å elongation of the C—C bond lengths and a fold angle of 10.4° that breaks the ring planarity. The nitrogen atoms of the $pda^{2-}$ ligands appear

(42) To avoid contamination with paramagnetic metal particles, sample manipulations for SQUID analysis were carried out with glass and plastic tools.

(43) Kahn, O. *Molecular Magnetism*; VCH Publishers: New York, 1993; Chapter 2.

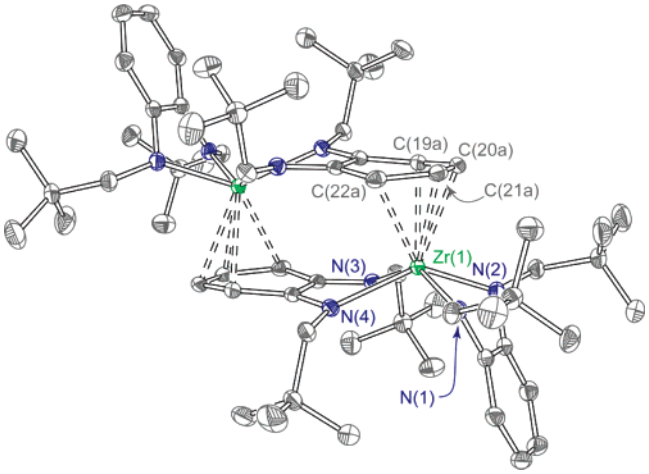


***Figure 2.*** Molecular structure of $[Zr(pda)_2]_2$ (**1b**). Solvent molecules and hydrogen atoms have been omitted for clarity. Ellipsoids are shown at 50% probability.

***Table 2.*** Selected Bond Lengths (Å) and Angles (deg) for $[Zr(pda)_2]_2$ (**1b**)

| bond lengths, Å | | bond angles, deg | |
|---|---|---|---|
| Zr(1)—N(1) | 2.1408(11) | N(1)—Zr(1)—N(2) | 78.64(4) |
| Zr(1)—N(2) | 2.1007(11) | N(1)—Zr(1)—N(3) | 143.62(4) |
| Zr(1)—N(3) | 2.2647(11) | N(1)—Zr(1)—N(4) | 92.07(4) |
| Zr(1)—N(4) | 2.2617(11) | N(3)—Zr(1)—N(4) | 70.56(4) |
| Zr(1)—C(19) | 2.7289(13) | C(20)—Zr(1)—C(21) | 31.71(5) |
| Zr(1)—C(20) | 2.5471(13) | C(20)—Zr(1)—N(2) | 85.56(5) |
| Zr(1)—C(21) | 2.5028(13) | C(20)—Zr(1)—N(3) | 108.55(4) |
| Zr(1)—C(22) | 2.6146(14) | C(21)—Zr(1)—N(1) | 85.34(4) |
| C(20)—C(21) | 1.380(2) | C(21)—Zr(1)— N(4) | 115.01(5) |

to be $sp^2$-hybridized (average sum of angles 357°); however, in the nonbridging $pda^{2-}$ ligands the plane of each $sp^2$-nitrogen is rotated by 32° from the plane of the arene ring. Similar distortions have been observed in phenylenediamide complexes of other $d^0$ complexes, and they serve to increase $\pi$-donation from the N lone pair to the empty metal $d_{xy}$ orbital.[44]

The THF adduct, **2**, crystallized in the *C*2/*c* space group from a chilled pentane solution and provided the molecular structure shown in Figure 3. Selected bond lengths and angles describing the zirconium coordination environment of **2** are included in Table 3. The zirconium center is best described as trigonal bipyramidal as indicated by an N(1)—Zr(1)—N(4) angle of 163.8° and a nearly trigonal equatorial plane (sum of angles 359.7°). As observed in the structure of **1b**, each nitrogen atom of **2** is $sp^2$-hybridized (sum of angles ∼ 358°), but the nodal plane for the unhybridized p orbital is rotated significantly from the plane of the aromatic ring (19−29°). Surprisingly, the oxygen atom of the coordinated THF molecule is also $sp^2$-hybridized (sum of angles 359.8°), which should allow the THF oxygen lone pair to act as a $\pi$-donor to the zirconium center.

X-ray diffraction studies of oxidation products **3a**−**c** revealed a zirconium complex in which halogen addition occurred at the metal center. Crystalline samples of oxidation products **3a**−**c** were obtained directly from reaction solutions stored at −35 °C; diffraction studies on these crystals provided the molecular structures shown in Figure 4 and the selected metrical

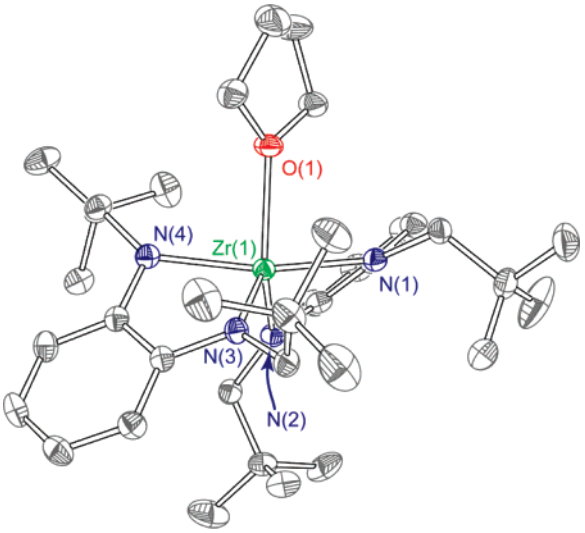


***Figure 3.*** Molecular structure of $Zr(pda)_2(THF)$ (**2**). Hydrogen atoms have been omitted for clarity. Ellipsoids are shown at 50% probability.

***Table 3.*** Selected Bond Lengths (Å) and Angles (deg) for $Zr(pda)_2(THF)$ (**2**)

| bond lengths, Å | | bond angles, deg | |
|---|---|---|---|
| Zr(1)—N(1) | 2.1298(15) | N(1)—Zr(1)—N(2) | 79.24(6) |
| Zr(1)—N(2) | 2.0583(15) | N(1)—Zr(1)—N(3) | 116.10(6) |
| Zr(1)—N(3) | 2.0576(15) | N(1)—Zr(1)—N(4) | 163.83(6) |
| Zr(1)—N(4) | 2.1625(15) | N(2)—Zr(1)—N(3) | 109.51(6) |
| Zr(1)—O(1) | 2.2797(13) | O(1)—Zr(1)—N(1) | 83.93(5) |
| | | O(1)—Zr(1)—N(2) | 131.83(5) |

parameters collected in Table 4.[45] In complexes **3a**−**c**, the zirconium center adopts a six-coordinate trigonal prismatic geometry with the halogen atoms in cis coordination sites. The Zr—X bond distances fall within the normal ranges for each halogen, though the X—Zr—X bond angles decrease with increasing halogen size: 86.061(15)° (**3a**), 85.061(18)° (**3b**), and 81.91(3)° (**3c**). The four nitrogen atoms of the chelating ligands complete the coordination environment around zirconium. Chart 1 shows the crystallographic bond lengths for the $pda^{2-}$ of **2** alongside the crystallographic bond lengths for the $disq^-$ ligands in compound **3a** (**3b** and **3c** display similar trends in $disq^-$ bond distances). Examination of the Zr—N bond distances in **3a**−**c** shows a significant elongation relative to the Zr—N bonds in compounds **1b** and **2**. This elongation is consistent with an oxidation of the chelating ligands to the monoanionic diimino-semiquinone form ($disq^-$).[46] Further evidence for the assignment of the ligand oxidation state is provided by comparison of the C—N and C—C bond distances in the $disq^-$ ligands of **3a**−**c** with the $pda^{2-}$ ligands of **2**. Localization of C—C and C═C bonds in the six-membered ring of each $disq^-$ ligand is evident from alternating bond distances. Contraction of the C—N bonds in **3a**−**c** is consistent with greater diimine character in the $disq^-$ ligand compared to the $pda^{2-}$ ligand of **2**.

Perhaps the most striking feature of the solid-state structures of **3a**−**c** is the orientation of the two $disq^-$ ligands. Each

(44) (a) Ison, E. A.; Cameron, T. M.; Abboud, K. A.; Boncella, J. M. *Organometallics* **2004**, *23*, 4070−4076. (b) Galindo, A.; Ienco, A.; Mealli, C. *Comments Inorg. Chem.* **2002**, *23*, 401−416. (c) Wang, S. S.; Abboud, K. A.; Boncella, J. M. *J. Am. Chem. Soc.* **1997**, *119*, 11990−11991.

(45) One iodide position, I(1), of **3c** was disordered significantly with a chloride ligand. The structure was modeled adequately with an iodide occupancy of 0.3 and a chloride occupancy of 0.7. The structure shown in Figure 4 and the data presented in Table 4 show only the partial occupancy iodide.

(46) Bhattacharya, S.; Gupta, P.; Basuli, F.; Pierpont, C. G. *Inorg. Chem.* **2002**, *41*, 5810−5816.

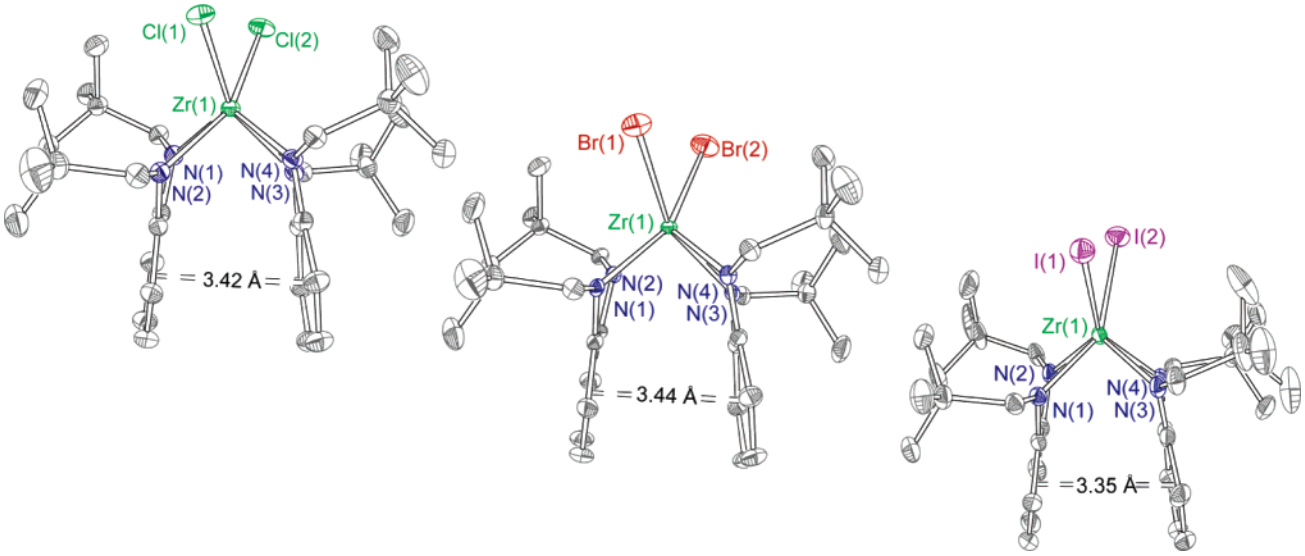


***Figure 4.*** Molecular structures of $ZrX_2(disq)_2$ (X = Cl, **3a**; X = Br, **3b**; X = I, **3c**). The distance shown between $disq^-$ ligands is measured between the centroid of each $C_6$ ring. Solvent molecules and hydrogen atoms have been omitted for clarity. Ellipsoids are shown at 50% probability.

***Table 4.*** Selected Bond Lengths (Å) and Angles (deg) for $ZrX_2(disq)_2$ (X = Cl, **3a**; X = Br, **3b**; X = I, **3c**)

| | $ZrCl_2(disq)_2$ (**3a**) | $ZrBr_2(disq)_2$ (**3b**) | $ZrI_2(disq)_2$ (**3c**) |
|---|---|---|---|
| Bond Lengths, Å | | | |
| Zr(1)—X(1) | 2.4708(4) | 2.6166(5) | 2.8878(4) |
| Zr(1)—X(2) | 2.4685(4) | 2.5996(5) | 2.7693(10) |
| Zr(1)—N(1) | 2.2141(12) | 2.210(3) | 2.200(3) |
| Zr(1)—N(2) | 2.1942(14) | 2.196(3) | 2.192(2) |
| Zr(1)—N(3) | 2.2233(12) | 2.223(3) | 2.201(3) |
| Zr(1)—N(4) | 2.1923(14) | 2.185(3) | 2.190(2) |
| Bond Angles, deg | | | |
| X(1)—Zr(1)—X(2) | 86.061(15) | 85.061(18) | 82.44(2) |
| N(1)—Zr(1)—N(2) | 72.52(5) | 72.64(11) | 73.24(9) |
| N(1)—Zr(1)—N(3) | 106.19(4) | 106.05(10) | 113.22(9) |
| N(1)—Zr(1)—N(4) | 65.45(5) | 75.78(11) | 76.72(9) |
| X(1)—Zr(1)—N(1) | 88.14(3) | 88.54(7) | 89.68(7) |
| X(1)—Zr(1)—N(4) | 92.73(4) | 93.17(8) | 88.47(7) |
| X(2)—Zr(1)—N(2) | 93.42(4) | 93.80(8) | 92.91(7) |
| X(2)—Zr(1)—N(3) | 87.98(3) | 88.30(8) | 88.41(7) |

***Chart 1***

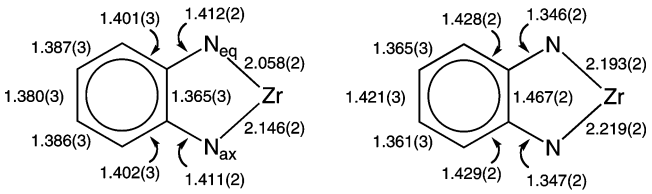


(a) $Zr(pda)_2(THF)$ (**2**) (b) $ZrCl_2(disq)_2$ (**3a**)

chelating ligand is bent down such that the rings are nearly parallel; the angle between the ring planes varies only slightly across the halide series, from 12.8° for the dichloride, to 13.3° for the dibromide, to 15.2° for the diiodide. The rings are canted slightly, such that the carbon atoms of one ring sit between two carbon atoms of the adjacent ring. Centroid−centroid distances of 3.42 Å (**3a**), 3.44 Å (**3b**), and 3.35 Å (**3c**) between the $disq^-$ rings are within the range observed for intramolecular stacking in other $\pi$-radical systems,[20,21] and inter-ligand N···N distances of ~2.7 Å are well within the standard van der Waals radius for two nitrogen atoms ($r_{vdW}$ = 155 pm).[47]

**Theoretical Studies.** Computational methods offer a mechanism for better understanding the electronic features giving rise to the properties observed for complexes **3a**−**c**. The presence of two open-shell, monoanionic $disq^-$ ligands in the coordination sphere of **3a**−**c** could lead to three possible electronic structure patterns. First, the two unpaired, ligand-based electrons may adopt a parallel orientation, displaying weak ferromagnetic coupling as reported previously for $d^0$ metal complexes with unpaired electrons located on semi-quinone ligands.[48] Second, the unpaired electrons may exhibit antiferromagnetic coupling to afford a singlet biradical ground state. Last, the structural orientation of the $disq^-$ ligands may allow for the formation of molecular orbitals that are delocalized over both $disq^-$ ligands. Pairing of the two $disq^-$ electrons into a single molecular orbital then would afford a closed-shell singlet ground state.

On the basis of the experimental evidence implicating a singlet ground state for complexes **3a**−**c**, first we set out to find an antiferromagnetic state in which one electron remains localized on each $disq^-$ ligand. Despite exhaustive attempts, including systematic orbital localization protocols that successfully located plausible antiferromagnetically coupled states in our previous studies,[36] we were unable to converge to a singlet biradical (i.e., open-shell) state for **3a**−**c**. Instead, all attempts to enforce an $S = 0$ spin state resulted in spontaneous convergence to a closed-shell singlet state in which the two electrons occupy the same spatial orbital that is delocalized fully over the two $disq^-$ ligands. After much experimentation, we concluded that an antiferromagnetic biradical state is not viable in the molecular structure observed for **3a**−**c**.

Calculations carried out enforcing an $S = 1$ spin state yielded a grossly different geometry than that observed in the solid-state structures of **3a**−**c**. Whereas the closed-shell singlet state

(47) Winter, M. WebElements Periodic Table Scholar Edition. http://www.webelements.com/webelements/scholar/ (accessed 17 Sept. 2007).
(48) (a) Bruni, S.; Caneschi, A.; Cariati, F.; Delfs, C.; Dei, A.; Gatteschi, D. *J. Am. Chem. Soc.* **1994**, *116*, 1388−1394. (b) Lange, C. W.; Conklin, B. J.; Pierpont, C. G. *Inorg. Chem.* **1994**, *33*, 1276−1283. (c) Adam, D. M.; Rheingold, A. L.; Dei, A.; Hendrickson, D. M. *Angew. Chem., Int. Ed. Engl.* **1993**, *32*, 391−392.

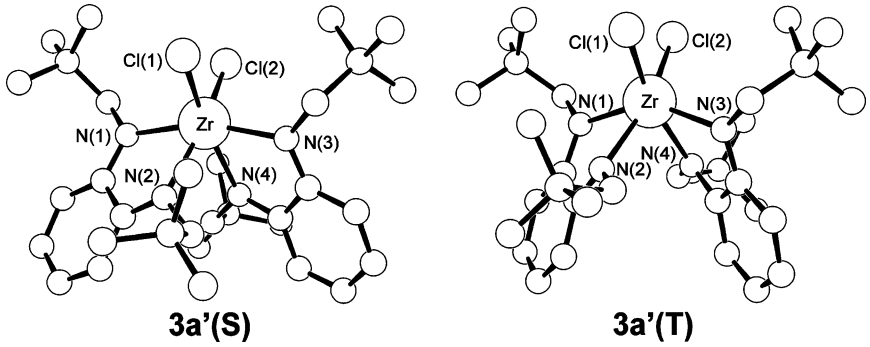


***Figure 5.*** Computed Structures of the **3a′(S)** and **3a′(T)**.

***Table 5.*** DFT-Computed Energies of the Different Possible Spin States of **3a**−**c**[a]

| | Δ*E*(SCF) | −(298.15 K)*S* | *G*(solv) | Δ*G*(sol) |
|---|---|---|---|---|
| **3a**(S) | 0.00 | −49.08 | −5.24 | 0.00 |
| **3a′**(S) | −0.67 | −50.91 | −4.42 | −1.98 |
| **3a′**(T) | +5.97 | −49.53 | −4.46 | +5.53 |
| **3b**(S) | 0.00 | −51.73 | −5.59 | 0.00 |
| **3b′**(S) | 0.00 | −52.72 | −4.81 | −0.40 |
| **3b′**(T) | +7.01 | −53.53 | −4.73 | +5.40 |
| **3c**(S) | 0.00 | −52.73 | −5.07 | 0.00 |
| **3c′**(S) | −0.23 | −54.16 | −4.15 | −0.88 |
| **3c′**(T) | 8.58 | −54.42 | −4.26 | +7.07 |

[a] Structural isomers are labeled as **3a**−**c′**, and (S) and (T) denote singlet and triplet spin states, respectively. All energies are given in kcal mol$^{-1}$.

obtained for **3a** affords a minimized geometry that is in good agreement with the experimental molecular structure shown in Figure 4, our calculations indicate that this geometry cannot accommodate a triplet state. Beginning with the crystallographic structure for **3a**, geometry optimization calculations in an enforced $S = 1$ spin state resulted in a repulsion of the $\pi$-stacked disq$^-$ ligands. This repulsion removed the $\pi-\pi$ interaction and led to a distorted octahedral coordination geometry for the Zr center in the $S = 1$ spin state. The fully optimized structure of the putative triplet state **3a′(T)** is shown in Figure 5.

Interestingly, the pseudo-octahedral geometry, **3a′(T)**, found for the triplet spin state of **3a** also supports a closed-shell singlet state. Figure 5 shows the minimized geometry for singlet **3a′-(S)**, with a pseudo-octahedral geometry. Analogous triplet and closed-shell singlet structural isomers **3b′** and **3c′** also were located for the Br and I substituted complexes **3b** and **3c**, respectively. A summary of the DFT-calculated energies for **3a**−**c(S)**, **3a**−**c′(S)**, and **3a**−**c′(T)** are shown in Table 5. According to DFT, the calculated singlet state structures **3a**−**c′(S)** were found to be slightly lower in energy than the experimentally observed structures **3a**−**c**. On the other hand, the triplet states **3a**−**c′(T)** were disfavored by 5−7 kcal mol$^{-1}$ in all cases. Inspection of the energy components given in Table 5 indicates that entropy and solvation corrections are essentially identical and the complexes **3a**−**c(S)** and **3a**−**c′(S)** also are electronically isoenergetic, with *E*(SCF) energy differences being −0.67 (Cl), 0.00 (Br), and −0.23 (I) kcal mol$^{-1}$.

The similarity in the DFT-calculated energies for the experimentally observed singlet states **3a**−**c(S)** and computationally located singlet states **3a**−**c′(S)** prompted a more thorough theoretical investigation of these species. The most striking difference between the geometries **3a**−**c(S)** and **3a**−**c′(S)** is in the orientation of the disq$^-$ ligands. In the experimentally observed trigonal-prismatic geometry, the two arene rings are within $\pi$-stacking distance. In the computationally minimized pseudo-octahedral geometry, no favorable interactions between the arene rings are possible. It is well-known that currently available DFT methods substantially underestimate van der Waals and dispersion forces[49] that would likely favor structure **3a**−**c(S)** over structure **3a**−**c′(S)**. Consistent with this notion, the DFT-calculated structures of **3a**−**c** display much longer distances between the arene rings of the disq$^-$ ligands than is observed experimentally: in the DFT-calculated structure of **3a** the centroid-to-centroid distance is 3.91 Å, whereas the experimentally observed centroid-to-centroid distance is 3.42 Å. To improve on this apparent failure of DFT to fully capture the structural features of **3a**, we have carried out a full geometry optimization at the MP2/cc-pVTZ(-f) level of theory, to better reproduce the influence of van der Waals and dispersion forces on the structures of **3a**−**c**. Using a slightly simplified model in which the *neo*-pentyl groups of the disq$^-$ ligands were replaced by methyl groups, the optimized MP2 structure shows a centroid-to-centroid distance of 3.52 Å for the disq$^-$ ligands. Energetically, the inclusion of these $\pi$-stacking effects gives rise to additional stabilization energy of 6.30 kcal mol$^{-1}$. Thus, we conclude that **3a(S)** is the lowest energy structure and that the **3a′(S)** and **3a′(T)** isomers are approximately 6 and 12 kcal mol$^{-1}$ higher in energy, respectively. We have also considered a rearrangement product, where the two halogen ligands occupy trans axial positions and the two disq ligands are in the equatorial plane. In all cases, these structures are 2−3 kcal/mol higher in electronic energy at the DFT level of theory. Thus, we estimate that these alternative structures are approximately 8 kcal/mol higher in energy than the $\pi$-stacked structures.

To synchronize further our theoretical and experimental work and to understand better the spectroscopic signature of **3a**, we computed the electronic excitation profile of complex **3a** using time-dependent DFT methods. In addition to the BP86-optimized full model that contains the *neo*-pentyl groups and the MP2-calculated small model where the *neo*-pentyl groups were simplified to methyl groups, we have also generated an "MP2-large model" by constraining the core fragment to that obtained from the methyl-model and re-optimizing the positions of the *neo*-pentyl groups at the DFT level of theory. This MP2-large model was employed to accurately simulate both the close $\pi$-stacked interaction of the disq$^-$ ligands and the large inductive effect of the electron-donating *neo*-pentyl groups. Geometry optimizations of the untruncated models at the MP2/cc-pVTZ-(-f) levels are technically not tractable, but the "MP2-large

(49) (a) Kristyan, S.; Pulay, P. *Chem. Phys. Lett.* **1994**, *229*, 175−180. (b) Wu, Q.; Yang, W. *J. Chem. Phys.* **2002**, *116*, 515−524. (c) Sinnokrot, M. O.; Sherrill, C. D. *J. Phys. Chem. A* **2004**, *108*, 10200−10207.

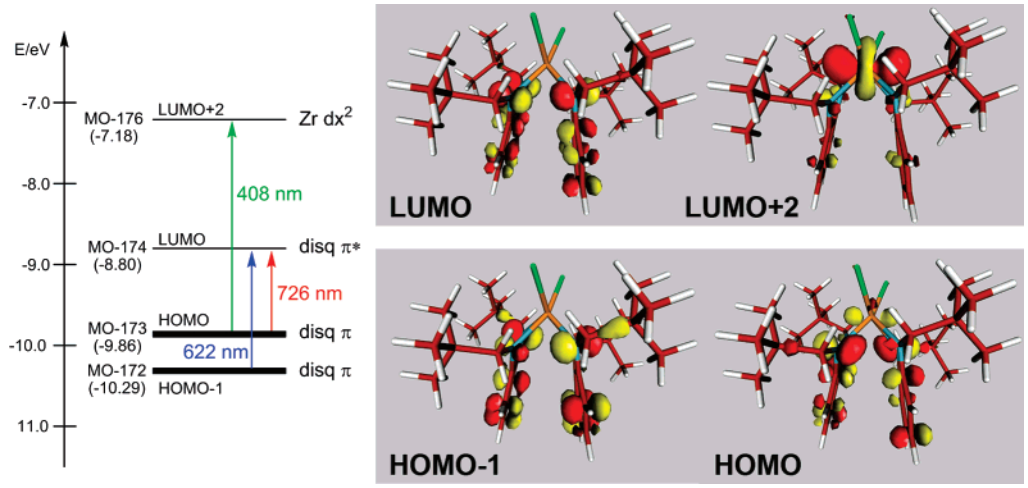


***Figure 6.*** Calculated electronic excitation profile and the isodensity plots (isodensity value = 0.05 a.u.) of the MOs involved in these transitions.

***Table 6.*** Experimental and TDDFT-Calculated Electronic Absorption Transitions for **3a** in DFT- and MP2-optimized Geometries[a]

| exp. | DFT | MP2-small | MP2-large | assignment |
|---|---|---|---|---|
| 443 | 394 | 396 | 408 | HOMO (disq-$\pi$) → LUMO+2 (Zr-$d_{x^2}$) |
| 660 | 684 | 609 | 622 | HOMO−1 (disq-$\pi$) → LUMO (disq-$\pi$*) |
| 730 | 774 | 697 | 726 | HOMO (disq-$\pi$) → LUMO (disq-$\pi$*) |

[a] All transitions are given in nanometers.

model" constitutes a reasonable compromise. The TDDFT results are summarized in Table 6. Whereas all three computational models gave reasonable predictions for the three low-energy transitions of **3a**, the transitions predicted using the MP2-large model clearly afforded the best agreement with the experimental absorption spectrum. The sensitivity of the simulated absorption wavelengths becomes clear upon inspection of the assignment of the MOs involved in the excitations. The primary MOs for the three excitations are shown in Figure 6.

As illustrated in Figure 6, the lowest-energy absorption for **3a** is a ligand-to-ligand charge transfer (LLCT) associated with the HOMO and LUMO. The lowest-energy transition is computed to be at 726 nm using the MP2-large model, which is in excellent agreement with the experimentally observed absorption at 730 nm. The DFT-geometry model and the truncated, MP2-methyl model afford less accurate results, predicting the lowest-energy transition at 774 and 697 nm, respectively. Both the HOMO and the LUMO are dominated by the $\pi$-orbitals of the disq$^-$ ligand, and the nitrogen donor atoms play an important role, as indicated by the large orbital coefficients of the N-based *p*-orbitals observed in both the HOMO and the LUMO of Figure 6. Furthermore, the HOMO and the LUMO correspond to in-phase and out-of-phase combinations of $\pi$-type fragment orbitals on each disq$^-$ ligand. As such, in Figure 6, the HOMO is labeled as "disq $\pi$" and the LUMO is labeled as "disq $\pi$*" to emphasize the $\pi-\pi$ bonding and $\pi-\pi$ antibonding character of these orbitals.

The antibonding character of the LUMO of **3a** provides an intuitive rationale for the structural distortion observed during geometry optimization with an enforced $S = 1$ spin state. In a triplet configuration, one electron must be moved from the "disq $\pi$" HOMO to the "disq $\pi$*" LUMO, eliminating any bonding-type interaction between the disq$^-$ ligands. Upon removal of this interaction, the zirconium complex relaxes to a pseudo-octahedral coordination geometry, which is accompanied by a flattening of the disq$^-$ ligands, as shown for **3a′(T)** in Figure 5.

The $\pi$ orbitals of the disq$^-$ ligands participate in both of the higher-energy electronic absorption transitions. The middle-energy transition, observed at 660 nm and calculated at 622 nm using the MP2-large model, can also be assigned as an LLCT transition with the HOMO-1 as the donor orbital and the LUMO as the accepting orbital. The highest-energy transition of interest is observed experimentally at 443 nm, and the MP2-large model located a ligand-to-metal charge transfer (LMCT) transition in this range, as shown in Figure 6. It involves the HOMO and a nonbonding $d_{x^2}$-orbital (LUMO+2), as shown in Figure 6. The good agreement between the computed and the experimental electronic spectra lends further support for our proposal that the ground state of **3a**−**c** is a closed-shell singlet state.

## Discussion

Oxidation of **1** or **2** with halogen reagents affords products **3a**−**c**, in which ligand-centered redox activity provides the reducing equivalents required to cleave the substrate bond and to form two new Zr−X bonds. The reaction that produced **3a**−**c** resembles a traditional oxidative addition reaction in that the addition of an oxidizing substrate occurs with the formation of two M−X bonds at the metal center. The derivation of the reducing equivalents from the redox-active ligand set, however, clearly differentiates it from a traditional oxidative addition pathway, which relies on the transfer of two valence electrons from the metal ion to the substrate during M−X bond formation. In the present reaction sequence, the two reducing equivalents that enabled the oxidative addition reaction to occur were provided by the dianionic pda$^{2-}$ ligands chelated to the zirconium center. This ligand oxidation was readily observed in the development of a dark blue-green solution during the reaction; moreover, X-ray diffraction studies on **3a**−**c** confirmed the disq$^-$ oxidation state for each ligand. Notably, the C−N bond distances of the ligand in the disq$^-$ oxidation state are contracted relative to those in the reduced pda$^{2-}$ oxidation state.

Similarly, localization of double bond character was readily observed within the phenyl rings as they take on cyclohexadiene character signaling oxidation to the disq$^-$ state. Such trends in bond distances are well established in high-resolution structures of transition metal complexes with semiquinone-type ligands.[46]

The orientation of the disq$^-$ ligands is strikingly similar across the halide series, **3a**−**c**, and results from a bonding-type interaction between singly occupied $\pi/\pi^*$ orbitals on each disq$^-$ ligand. Calculations on the parent pda$H_2$ molecule show a HOMO of $\pi/\pi^*$ character that is delocalized over the two nitrogen atoms and six carbon atoms of the phenyl ring; one-electron oxidation to the disq$^-$ state leaves a single unpaired electron in this molecular orbital. In the trigonal prismatic structure of **3a**−**c**, the disq$^-$ ligands are in a nearly parallel arrangement so that in-phase and out-of-phase linear combinations of the ligand-only SOMOs form bonding and antibonding interactions, respectively. The addition of two electrons to the in-phase orbital combination in the ground state of **3a**−**c** results in a bonding interaction that stabilizes this arrangement of the disq$^-$ ligands. Computationally we have estimated this interaction to provide ∼6 kcal mol$^{-1}$ of stabilization relative to two separated radical disq$^-$ ligands. Accordingly, the ground state electron configuration of **3a**−**c** is best described as a closed-shell singlet, and consistent with this proposal, temperature-dependent magnetic measurements clearly show a singlet ground state for **3a**−**c**. Conceptually, this interaction may be thought of as a dimer of two disq$^-$ radicals. Similar interactions have been proposed for the temperature-dependent dimerization of phenalenyl radicals.[19] Here, the SOMOs of two phenalenyl radicals interact to form in-phase and out-of-phase linear combinations, resulting in a diamagnetic ground state for the phenalenyl dimer. Formation of the dimer is temperature dependent and was readily observed by loss of the EPR signal at low temperatures.

The temperature dependence of the effective magnetic moment and the electronic absorption spectra of **3a**−**c** allow for the experimental determination of the one- and two-electron energy terms for the bonding interactions between the two disq$^-$ radicals. As shown in Figure 6, the HOMO and LUMO of **3a**−**c** have little contribution from the bridging zirconium center and thus can be approximated as pure $\pi$-stacked bonding and antibonding combinations of the singly occupied disq$^-$ orbitals. In such weakly interacting systems, the four electronic states shown in Figure 7 have been used both in valence-bond[50] and molecular-orbital[51] theories to describe the electronic structure of the two-electron interaction. In the molecular orbital formalism, this model was first applied to the $\sigma$ bond of "stretched" dihydrogen[52] and the $\pi$ bond of twisted ethylene.[53] The $\delta$ bond of quadruply bonded metal dimers has provided a framework to evaluate experimentally the complete four-state manifold.[54] More recently, one- and two-electron energies for a molybdenum−molybdenum $\pi$-bond have been determined experimentally.[55] Assuming an idealized $C_{2v}$ geometry for **3a**−**c**, the

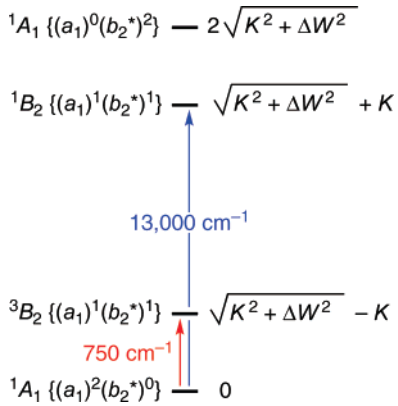


***Figure 7.*** Energies of the lowest electronic states of $ZrX_2(disq)_2$ (X = Cl, **3a**; X = Br, **3b**; X = I, **3c**); 2$K$ is the two-electron exchange energy and 2$\Delta W$ is the one-electron energy separating the bonding and antibonding orbital combinations.

electronic states of Figure 7 carry the symmetry labels $^1A_1$ $(a_1)^2(b_2)^0$, $^3B_2$ $(a_1)^1(b_2)^1$, $^1B_2$ $(a_1)^1(b_2)^1$, and $^1A_1$ $(a_1)^0(b_2)^2$. According to the formalism used by Cotton and Nocera,[54a] the exchange energy for the two electrons, $K$, may be determined directly from the difference between the energies of the $^3B_2$ and $^1B_2$ states derived from the two $(a_1)^1(b_2)^1$ electron configurations ($2K = \Delta E = E(^1B_2) - E(^3B_2)$). In the case of **3a**−**c**, the $^3B_2$ energy can be crudely approximated from the temperature dependence of the magnetic susceptibility (∼750 cm$^{-1}$) and the $^1B_2$ energy can be approximated as the lowest-energy band in the electronic absorbance spectrum (∼13 000 cm$^{-1}$). These approximations provide an experimental estimate of 6000 cm$^{-1}$ for the exchange energy, $K$. The interaction energy for the two disq$^-$ ligands (i.e., the one-electron HOMO−LUMO gap for **3a**−**c**, $\Delta W = E(b_2) - E(a_1)$) is estimated at $\Delta W = 3000$ cm$^{-1}$.

Intuitively, the estimates of the $K$ and $\Delta W$ are reasonable for complexes **3a**−**c**. Examination of the metrical parameters in the solid-state structures of **3a**−**c** show a centroid-to-centroid distance of ∼3.4 Å across the halide series (see Figure 4). Because the disq$^-$ ligands are not perfectly parallel, the nitrogen atoms of the disq$^-$ ligands are closer at ∼2.7 Å (N(1)···N(4) and N(2)···N(3)), and while this is well outside of the normal N—N bonding range, it is within the sum of the van der Waals radii for two nitrogen atoms (3.10 Å). This long-distance interaction between the disq$^-$ ligands affords small overlap between the ligand SOMOs and therefore a small energy separation between the bonding and the antibonding combinations of orbitals (i.e., a small $\Delta W$). The exchange energy, $K$, corresponds to the energy required to transfer an electron from one disq$^-$ ligand to the other. In effect, such an electron transfer would produce an excited-state electronic structure with one dianionic pda$^{2-}$ ligand and one neutral diq ligand (diq = *N*,*N*-di-*neo*-pentyl-1,2-diiminoquinone). Such symmetric zwitterionic electronic states are normally observed only as transient intermediates, and in this case the high energy of such a state is reflected in a relatively large value for the exchange energy.

## Conclusions

A halogen oxidative−addition-like reaction provides access to new zirconium(IV) complexes with two disq$^-$ ligands. Structural and spectroscopic studies clearly indicate the par-

(50) Heitler, W.; London, F. *Z. Phys.* **1927**, *44*, 455−472.
(51) Coulson, C. A.; Fischer, I. *Philos. Mag.* **1949**, *40*, 386−393.
(52) Mulliken, R. S. *Phys. Rev.* **1936**, *50*, 1017−1027.
(53) Mulliken, R. S. *Phys. Rev.* **1932**, *41*, 751−758.
(54) (a) Cotton, F. A.; Nocera, D. G. *Acc. Chem. Res.* **2000**, *33*, 483−490. (b) Engebretson, D. S.; Graj, E. M.; Leroi, G. E.; Nocera, D. G. *J. Am. Chem. Soc.* **1999**, *121*, 868−869. (c) Cotton, F. A.; Eglin, J. L.; Hong, B.; James, C. A. *J. Am. Chem. Soc.* **1992**, *114*, 4915−4917. (d) Hopkins, M. D.; Zietlow, T. C.; Miskowski, V. M.; Gray, H. B. *J. Am. Chem. Soc.* **1985**, *107*, 510−512.
(55) Rosenfeld, D. C.; Wolczanski, P. T.; Barakat, K. A.; Buda, C.; Cundari, T. R. *J. Am. Chem. Soc.* **2005**, *127*, 8262−8263.

ticipation of ligand-based redox in facilitating the addition of the halogen substrate to the metal center. In this way, the redox-active $pda^{2-}$ ligands enable a reaction that would be otherwise impossible for a metal center with a $d^0$ electron count.

The oxidized products **3a**−**c** provided an intriguing platform to investigate the interaction of two $\pi$-radical $disq^-$ ligands. In this case a formal zirconium(IV) metal center acted as an effective template for a weak two-electron interaction or "bond" between $disq^-$ ligands. Experimentally this interaction produces a singlet ground state with a thermally accessible triplet excited state and a zwitterionic excited state accessible upon irradiation with visible light (a second zwitterionic state should be accessible upon two-photon absorption). The electronic structure for **3a**−**c** stands in stark contrast both to late transition metal complexes and to other $d^0$ metal complexes with redox-active ligands. Gray and co-workers originally proposed a *biradical* singlet ground state electronic structure for nickel(II) complexes with two radical ligands.[56] Recent studies by Wieghardt and co-workers show that the filled $d_{xz}$ and $d_{yz}$ orbitals of the square-planar $d^8$ complexes provide the super-exchange pathway for anti-ferromagnetic coupling.[2a,57] Weak ferromagnetic coupling has been observed for $d^0$ metal complexes with two radical ligands,[48] and theoretical studies show that orthogonal, empty, metal orbitals mediate the exchange interactions in these triplet, biradical complexes.[58] In the case of **3a**−**c**, there is no biradical character in the ground state because of the direct overlap between the singly occupied $disq^-$ orbitals. This closed-shell electronic structure may be a critical feature favoring two-electron rather than one-electron radical reactivity from a metal−bis(semiquinone) platform. Further experimental and computational studies are currently underway to investigate this hypothesis.

**Acknowledgment.** We thank the NSF (CHE-0645685 to A.F.H. and CHE-0645381 to M.-H.B.) for financial support. M.-H.B. is a Cottrell Scholar of the Research Corporation and an Alfred P. Sloan Fellow of the Alfred P. Sloan Foundation.

**Supporting Information Available:** Crystallographic data for **1b**, **2**, **3a**−**c** (CIF), SQUID data for **3a**−**c**, and computational details. This material is available free of charge via the Internet at http://pubs.acs.org.

JA077337M

(56) Steifel, E. I.; Waters, J. H.; Billig, E.; Gray, H. B. *J. Am. Chem. Soc.* **1965**, *87*, 3016−3017.

(57) (a) Herebian, D.; Wieghardt, K. E.; Neese, F. *J. Am. Chem. Soc.* **2003**, *125*, 10997−11005. (b) Bachler, V.; Olbrich, G.; Neese, F.; Wieghardt, K. *Inorg. Chem.* **2002**, *41*, 4179−4193.

(58) (a) Bencini, A.; Ciofini, I.; Giannasi, E.; Daul, C. A.; Doclo, K. *Inorg. Chem.* ***1998***, *37*, 3719−3725. (b) Ciofini, I.; Daul, C. A. *Coord. Chem. Rev.* **2003**, *238*−*239*, 187−209.